Available online at www.sciencedirect.com
SCIENCE DIRECT®
International Journal of Thermal Sciences 42 (2003) 199–208
International Journal of Thermal Sciences
www.elsevier.com/locate/ijts

Effects of the thermal boundary conditions at the sidewalls upon natural convection in rectangular enclosures heated from below and cooled from above

Massimo Corcione

Dipartimento di Fisica Tecnica, Università degli Studi di Roma "La Sapienza", via Eudossiana 18, 00184 Rome, Italy

Received 11 January 2002; accepted 4 March 2002

Abstract

Steady laminar natural convection in air-filled, 2-D rectangular enclosures heated from below and cooled from above is studied numerically for a wide variety of thermal boundary conditions at the sidewalls. A specifically developed numerical model based on the SIMPLER algorithm is used for the solution of the mass, momentum and energy transfer governing equations. Simulations are performed for several values of both the width-to-height aspect ratio of the enclosure in the range between 0.66 and 8, and the Rayleigh number based on the cavity height in the range between 10^3 and 10^6, whose influence upon the flow patterns, the temperature distributions and the heat transfer rates are analyzed and discussed. Comparisons among the different thermal configurations considered are reported. In particular, with reference to the typical configuration wherein the sidewalls are adiabatic, it is found that the heat transfer effectiveness of the bottom wall increases (or slightly decreases) as each adiabatic sidewall is replaced by a cooled (or a heated) sidewall. An opposite behaviour is observed for the top wall. The heat transfer rate results obtained are expressed through dimensionless correlation-equations.

Keywords: Natural convection; Rectangular enclosures; Heating from below; Sidewall boundary conditions; Numerical analysis; Dimensionless correlations

1. Introduction

Natural convection in enclosures has been extensively studied both experimentally and numerically, being of considerable interest in many engineering and science applications, e.g., collection of solar energy, operation and safety of nuclear reactors, energy efficient design of buildings and rooms, effective cooling of electronic components and machinery.

Most of the papers in this field are substantially oriented toward the study of rectangular enclosures wherein the heat flow is typically unidirectional, i.e., the buoyancy is induced by imposing a heating either from the side (for conventional convection) or from below (for thermal instabilities), as also reported in the general review works on natural convection in closed cavities by Catton [1] and by Ostrach [2]. Although many different geometries and boundary conditions are present in practice, little work has been carried out for more complex shapes of the enclosure and for multidirectional heat flows across the cavity, such as the case when the assigned thermal gradients are neither simply horizontal or vertical, that, as pointed out by Ostrach [2], may be rather seen as an exception.

Leaving aside studies related to non-simple geometries—see, e.g., Ciofalo and Karayiannis [3] and Chinnokotla et al. [4]—and to mixed temperature and/or heat flux conditions on the same boundary wall—see, e.g., November and Nansteel [5] and Valencia and Frederick [6]—, among the papers dealing with multidirectional heat fluxes across rectangular enclosures available in the literature, a specific interest is here focused on those wherein a bottom heating and/or a top cooling are involved.

Studies on natural convection in rectangular enclosures heated from below and cooled along a single side or both sides have been carried out respectively by Anderson and Lauriat [7] and by Ganzarolli and Milanez [8]. More recently the case of heating from one side and cooling from the top has been analyzed by Aydin et al. who investigated both the

E-mail address: massimo.corcione@uniroma1.it (M. Corcione).

1290-0729/02/$ – see front matter
PII: S1290-0729(02)00019-4

Nomenclature

A	aspect ratio of the enclosure, $= L/H$		
g	gravitational acceleration	$\mathrm{m\cdot s^{-2}}$	
H	height of the enclosure	m	
h	coefficient of convection	$\mathrm{W\cdot m^{-2}\cdot K^{-1}}$	
k	thermal conductivity	$\mathrm{W\cdot m^{-1}\cdot K^{-1}}$	
L	length of the enclosure	m	
Nu	average Nusselt number, $= hH/k$		
P	dimensionless pressure		
p	pressure	Pa	
Pr	Prandtl number, $= \nu/\alpha$		
Q	heat transfer rate	W	
Ra	Rayleigh number based on the cavity height, $= g\beta(T_H - T_C)H^3Pr/\nu^2$		
T	temperature	K	
U	dimensionless horizontal velocity component		
V	dimensionless vertical velocity component		
u	horizontal velocity component	$\mathrm{m\cdot s^{-1}}$	
v	vertical velocity component	$\mathrm{m\cdot s^{-1}}$	
X	dimensionless horizontal coordinate		
Y	dimensionless vertical coordinate		
x	horizontal coordinate	m	
y	vertical coordinate	m	

Greek symbols

α	thermal diffusivity	$\mathrm{m^2\cdot s^{-1}}$
β	coefficient of volumetric thermal expansion	$\mathrm{K^{-1}}$
ν	kinematic viscosity	$\mathrm{m^2\cdot s^{-1}}$
θ	dimensionless temperature	
ρ	density	$\mathrm{kg\cdot m^{-3}}$
Ψ	dimensionless stream function	

Subscripts

C	cold
h	horizontal boundary surface
H	hot
max	maximum value
v	vertical boundary surface
m	mean value

effects of Prandtl number upon heat and momentum transfer inside square cavities [9] and the influence of the aspect ratio for air-filled, rectangular enclosures [10].

As concerns situations wherein a simultaneous heating from below and cooling from above is considered, most of the work done deals mainly with mixed cavity natural convection in square geometries. This is, e.g., the case of the studies carried out by Shiralkar and Tien [11], who investigated the effects of stabilizing and destabilizing vertical thermal gradients upon natural convection in a sidewall-heated, air-filled, square enclosure for Rayleigh numbers up to 10^6, and by Kirkpatrick and Bohn [12], who conducted heat transfer measurements at Rayleigh numbers of the order of 10^{10} in a water-filled, cubical enclosure. On the contrary, despite the importance in practical applications, a smaller attention has been paid to either taller or shallower rectangular geometries, as well as to other boundary conditions at the lateral walls, i.e., different combinations of heated, cooled and adiabatic sidewalls.

In this framework, the aim of the present paper is to investigate natural convection in rectangular cavities simultaneously heated from below and cooled from above with several specified thermal boundary conditions at the sidewalls. The study is conducted numerically under the assumption of steady laminar flow, for different values of both the width-to-height aspect ratio of the enclosure in the range between 0.66 and 8, and the Rayleigh number based on the cavity height in the range between 10^3 and 10^6, whose influence upon the flow patterns, the temperature distributions and the heat transfer rates are analyzed and discussed.

2. Mathematical formulation

An air-filled, rectangular enclosure of height H and length L is heated from the bottom, kept at temperature T_H, and cooled from the top, maintained at temperature T_C, as sketched in Fig. 1, where the coordinate system adopted is also represented. As far as the sidewalls are concerned, the following thermal configurations reported in Fig. 2 are considered: (1) both sidewalls adiabatic, denoted

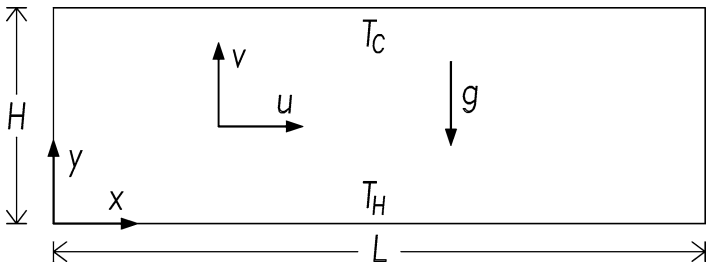

Fig. 1. Sketch of the geometry and coordinate system of the cavity.

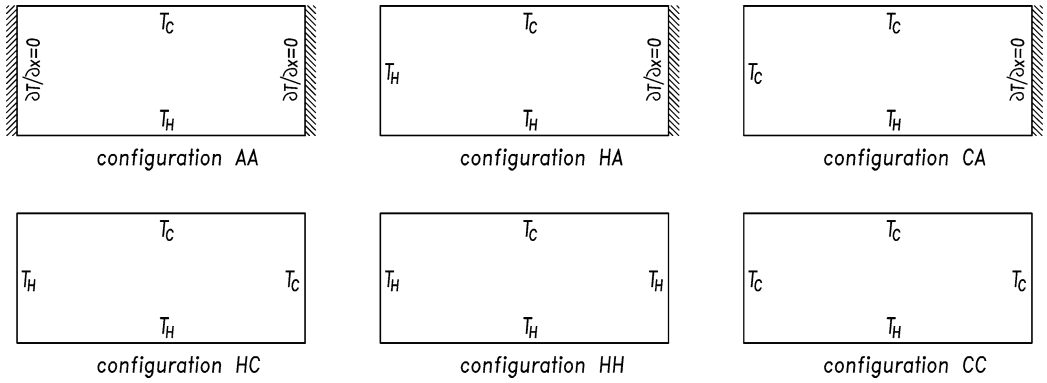

Fig. 2. Thermal configurations of the cavity.

as AA; (2) one sidewall heated at temperature T_H and one sidewall adiabatic, denoted as HA; (3) one sidewall cooled at temperature T_C and one sidewall adiabatic, denoted as CA; (4) one sidewall heated at temperature T_H and one sidewall cooled at temperature T_C, denoted as HC; (5) both sidewalls heated at temperature T_H, denoted as HH; (6) both sidewalls cooled at temperature T_C, denoted as CC.

The buoyancy-driven flow is considered to be two-dimensional, steady and laminar. The fluid is assumed to be incompressible, with constant physical properties and negligible viscous dissipation. The buoyancy effects upon momentum transfer are taken into account through the Boussinesq approximation.

Once the above assumptions are employed into the conservation equations of mass, momentum and energy, and the following dimensionless variables are introduced:

$$X = \frac{x}{H}, \qquad Y = \frac{y}{H} \tag{1}$$

$$U = \frac{u}{(\nu/H)}, \qquad V = \frac{v}{(\nu/H)}, \qquad P = \frac{p+\rho g y}{\rho(\nu/H)^2} \tag{2}$$

$$\theta = \frac{(T-T_m)}{(T_H-T_C)} \quad \text{with } T_m = \frac{T_H+T_C}{2} \tag{3}$$

the following set of governing equations is obtained:

$$\frac{\partial U}{\partial X} + \frac{\partial V}{\partial Y} = 0 \tag{4}$$

$$U\frac{\partial U}{\partial X} + V\frac{\partial U}{\partial Y} = -\frac{\partial P}{\partial X} + \left(\frac{\partial^2 U}{\partial X^2} + \frac{\partial^2 U}{\partial Y^2}\right) \tag{5}$$

$$U\frac{\partial V}{\partial X} + V\frac{\partial V}{\partial Y} = -\frac{\partial P}{\partial Y} + \left(\frac{\partial^2 V}{\partial X^2} + \frac{\partial^2 V}{\partial Y^2}\right) + \frac{Ra}{Pr}\theta \tag{6}$$

$$U\frac{\partial \theta}{\partial X} + V\frac{\partial \theta}{\partial Y} = \frac{1}{Pr}\left(\frac{\partial^2 \theta}{\partial X^2} + \frac{\partial^2 \theta}{\partial Y^2}\right) \tag{7}$$

where $Ra = g\beta(T_H - T_C)H^3 Pr/\nu^2$ is the Rayleigh number based on the cavity height.

The thermal boundary conditions assumed are $\theta = 1/2$ at the bottom, $\theta = -1/2$ at the top, and: (a) $\partial\theta/\partial X = 0$ at any adiabatic sidewall; (b) $\theta = 1/2$ at any heated sidewall; (c) $\theta = -1/2$ at any cooled sidewall. Finally, as far as the velocity boundary conditions are concerned, the no-slip condition $U = V = 0$ is assumed along the four boundary walls.

3. Solution procedure

Finite difference equations are derived by integrating the governing differential equations (4)–(7) over an elementary control volume. A power law scheme is adopted for the convection–diffusion formulation. Pressure-velocity coupling is handled by using the SIMPLER algorithm (semi implicit method for pressure linked equations revised) described in full details by Patankar [13]. The discretized equations obtained are solved iteratively, using a line-by-line application of the Thomas algorithm. The non-linear coefficients are substituted successively with updated values. Underrelaxation is used to ensure the convergence of the iterative procedure, and the block correction scheme illustrated by Settari and Aziz [14] is incorporated to accelerate the convergence rate.

The solution domain is covered with a non-equidistant grid, having a concentration of grid lines near the boundary surfaces and a uniform spacing in the interior of the cavity. Furthermore, since multicell flow structures are expected, especially at the largest width-to-height aspect ratios investigated, and the location of the cell interfaces is not known a priori, a fine mesh spacing is used everywhere in the horizontal direction.

The solution is considered to be fully converged when the maximum absolute value of the mass source and the percent changes of the dependent variables at any grid-node from iteration to iteration are smaller than a prescribed value, i.e., 10^{-4} and 10^{-5}, respectively. In addition, the percent difference between the incoming and outcoming heat transfer rates is used as a further indication of the accuracy of the solution achieved.

After convergence is attained, the average Nusselt number Nu_h of each horizontal boundary wall and the average Nusselt number Nu_v of each vertical boundary wall, are calculated:

$$Nu_h = \frac{|Q_h|H}{kL(T_H - T_C)} = -\frac{1}{A}\int_0^A \left.\frac{\partial\theta}{\partial Y}\right|_{\text{wall}} \mathrm{d}X \tag{8}$$

$$Nu_v = \frac{|Q_v|}{k(T_H - T_C)} = -\int_0^1 \left.\frac{\partial\theta}{\partial X}\right|_{\text{wall}} \mathrm{d}Y \tag{9}$$

where $A = L/H$ is the width-to-height aspect ratio of the enclosure. The temperature gradients at the walls are evaluated by assuming a second-order temperature profile among each wall node and the next two interior nodes. The integrals are approximated by the trapezoid rule.

Grid-dependence tests have been conducted for all the configurations investigated. In particular, a special attention has been paid to the grid size dependent effect of the temperature discontinuity at the intersection of differently heated horizontal and vertical boundary walls upon the local (and then the overall) Nusselt numbers, that tend to increase significantly as the mesh spacing at the corner is reduced. Currently, the simplest way of handling the problem is assuming the average temperature of the two walls at the corner and keeping the adjacent grid-nodes at the respective wall temperatures. On the other hand, as shown by Ganzarolli and Milanez [8], this procedure is still grid-dependent unless a sufficiently refined mesh spacing is adopted. According to this result, once any corner formed by the intersection of two differently heated boundary walls is assumed at the average temperature of the adjacent walls, the optimal grid size obtained for each configuration analyzed corresponds to the mesh spacing over which further grid refinements do not produce any noticeable modification of both the heat transfer rates and the predicted flow field. Namely, when the percent changes of the average Nusselt numbers Nu_h and Nu_v defined above, as well as those of the maximum horizontal and vertical dimensionless velocity components at assigned vertical and horizontal sample planes across the cavity, are smaller than a given accuracy value, i.e., 1%. Typical numbers of nodal points adopted are 33×33 for the square cavity and 251×33 for the cavity with aspect ratio $A = 8$.

Furthermore, in order to validate the numerical code specifically developed for the present study, the solutions obtained for $Ra = 10^3$–10^6 in a square cavity with differently heated sidewalls and adiabatic top and bottom walls have been compared with the benchmark results of de Vahl Davis [15], showing a meaningfully good agreement. In particular, the average Nusselt numbers throughout the cavity, as well as the maximum horizontal and vertical velocity components respectively on the vertical and the horizontal midplane of the enclosure, are within 1–2% of the benchmark data. In addition, a very good agreement in the same range of the Rayleigh number has also been obtained between the results relevant to the HC configuration applied to a square enclosure and the heat transfer rate numerical solutions obtained by Shiralkar and Tien [11].

4. Results and discussion

Numerical simulations are performed for $Pr = 0.71$ (air is the working fluid) and different values of both the Rayleigh number in the range $10^3 \leqslant Ra \leqslant 10^6$ and the aspect ratio of the cavity in the range $0.66 \leqslant A \leqslant 8$.

In order to point out the influence of Ra and A upon the flow structure type and the temperature distributions throughout the cavity, sample local results are reported in terms of isotherms and streamlines. In all the isotherm plots, the contour lines correspond to equispaced values of the dimensionless temperature θ in the range between -0.5 and $+0.5$. In all the streamline plots, the contour lines correspond to equispaced absolute values of the normalized dimensionless stream function $\Psi/\Psi_{\max}$ in the range between 0 and 1, where the dimensionless stream function Ψ is defined as usual through $U = \partial\Psi/\partial Y$ and $V = -\partial\Psi/\partial X$.

Actually, since the isotherm and streamline contour plots of configurations CC and HH, as well as those of configurations CA and HA, have resulted symmetric about the horizontal midplane of the cavity, which means that:

$$\theta_{\mathrm{CC}}(X,Y) = -\theta_{\mathrm{HH}}(X,1-Y) \quad \text{and} \quad \theta_{\mathrm{CA}}(X,Y) = -\theta_{\mathrm{HA}}(X,1-Y) \tag{10}$$

$$U_{\mathrm{CC}}(X,Y) = U_{\mathrm{HH}}(X,1-Y) \quad \text{and} \quad U_{\mathrm{CA}}(X,Y) = U_{\mathrm{HA}}(X,1-Y) \tag{11}$$

$$V_{\mathrm{CC}}(X,Y) = -V_{\mathrm{HH}}(X,1-Y) \quad \text{and} \quad V_{\mathrm{CA}}(X,Y) = -V_{\mathrm{HA}}(X,1-Y) \tag{12}$$

the local results of configurations CC and CA are omitted for the sake of brevity.

4.1. Effects of the Rayleigh number

Isotherm and streamline contour plots relevant to the basic configuration AA, as well as to configurations HA, HC and HH, are represented in Fig. 3 for the cavity aspect ratio $A = 2$ and Rayleigh numbers $Ra = 10^4$–10^6.

It may be seen that for configurations AA and HH and for configuration HC the flow field consists respectively of two counterrotating cells, symmetric about the vertical midplane of the cavity, and of a single cell, symmetric about the center of the enclosure, that remain stable as the Rayleigh number increases. In addition, for configuration AA at $Ra = 10^6$ the formation of two secondary small cells near both top corners of the cavity is detected.

On the contrary, the flow field of configuration HA is asymmetric, tending to evolve from two counterrotating cells to a single-cell flow pattern as Ra increases up to 10^6. In detail, as the Rayleigh number increases starting from 10^4, the cell located closer to the heated sidewall expands toward the adiabatic sidewall, thus compressing the other cell that simply vanishes at $Ra = 10^6$.

As far as the isotherms are concerned, at $Ra = 10^3$ (not represented) they are very close to the typical tempera-

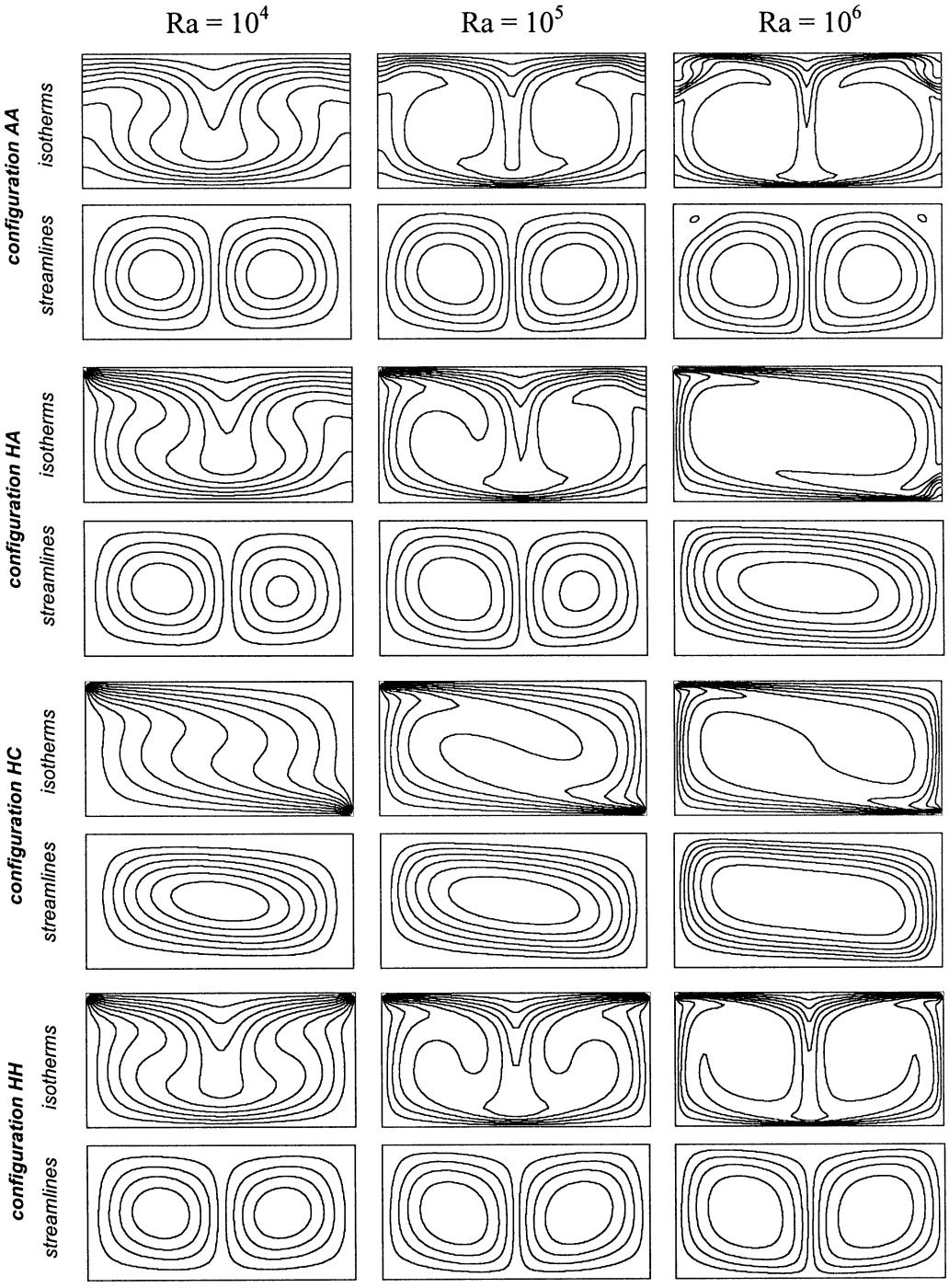

Fig. 3. Isotherms and streamlines for $A = 2$ and $10^4 \leqslant Ra \leqslant 10^6$.

ture distribution that corresponds to the limit of pure conduction. As the Rayleigh number increases, and thus also the buoyancy-driven circulation inside the cavity, a progressive warping around the centers of rotation and a more and more pronounced compression of the isotherms toward the boundary surfaces of the enclosure do occur. In particular, at $Ra = 10^5$ the temperature gradients near both the heated and the cooled walls start to be large enough to suggest the development of thermal boundary layers, whilst at $Ra = 10^6$ relatively stagnant core regions of fluid at uniform temperature are observed. The temperature gradient on the heated floor, and then the corresponding heat flux, is maximum near the centre, tending to decrease toward both bottom corners, for configurations AA, HA and HH. On the contrary, for configuration HC the temperature gradient is maximum near the cooled sidewall, tending to decrease toward the heated one. Practically opposite distributions may be observed on the cooled ceiling. As concerns the local heat flux from any

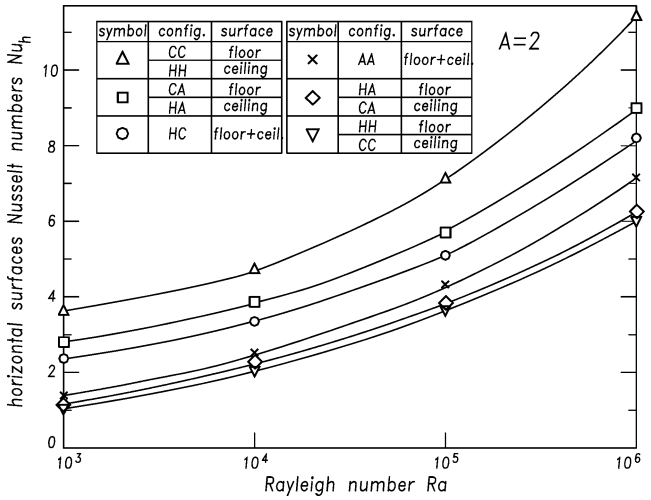

Fig. 4. Distributions of Nu_h vs. Ra for $A = 2$ (all configurations analyzed).

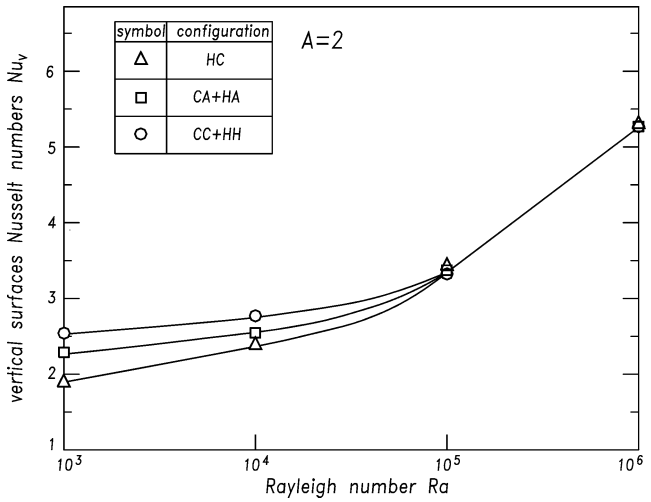

Fig. 5. Distributions of Nu_v vs. Ra for $A = 2$ (all configurations analyzed).

heated or cooled sidewall, leaving aside the close proximity of their intersection with the cooled ceiling or the heated floor of the cavity, for all the configurations analyzed the temperature gradient is maximum in the middle portion of the wall, tending to decrease toward the bottom and top corners.

The effects upon the heat transfer rates are pointed out in Figs. 4 and 5, where the distributions of the average Nusselt number of respectively the horizontal boundary surfaces and the vertical heated or cooled sidewalls of each thermal configuration of the enclosure with $A = 2$ are plotted vs. the Rayleigh number.

Besides the expected increase of the Nusselt numbers with Ra, it seems worthwhile noticing that, with respect to the reference configuration AA, the heat transfer rate from the heated floor (or the cooled ceiling) increases meaningfully as each vertical adiabatic boundary surface is replaced by a cooled (or a heated) sidewall, that is the case of configurations CA and CC (or HA and HH). As a matter of fact, while in the CA (or HA) configuration it is possible to transfer heat from the hot floor (or the cold ceiling) directly to the cold (or hot) sidewall, this is not permitted in the AA configuration, where the "crossing" of the whole cavity is required. For the same reason even higher heat transfer from the floor (or the ceiling) is produced in the CC (or HH) configuration.

On the contrary, only small decreases in the heat transfer rate from the heated floor (or the cooled ceiling) are observed when the replacement of each adiabatic sidewall is carried out through a heated (or a cooled) sidewall, that is the case of configurations HA and HH (or CA and CC). This may be explained by considering that when the sidewalls are either heated (or cooled) or insulated the lateral heat transfer from the hot floor (or the cold ceiling) is not permitted, thus implying that the overall thermal resistance is practically the same for the reference configuration AA and for both configurations HA and HH (or CA and CC). On the other hand, the heat exchanged by the portion of the hot floor (or the cold ceiling) located in the close vicinity of a heated (or a cooled) sidewall is smaller than the heat exchanged by the same portion of the floor when an adiabatic sidewall is used. It then follows that slight decreases in the heat transfer rates from the bottom wall (or the top wall) are to be expected when passing from configuration AA to configurations HA and HH (or CA and CC).

According to the fact that the positive effect of a cooled (or a heated) sidewall is more pronounced than the negative effect of a heated (or a cooled) sidewall, increases in the heat transfer rates from the horizontal boundary walls of the enclosure are indeed observed when both vertical adiabatic surfaces are replaced by one heated and one cooled sidewall, that is the case of configuration HC.

Finally, as far as the heat transfer rates from the vertical sidewalls are concerned, it may be noticed that starting from $Ra = 10^5$, within the accuracy of the numerical model all the thermal configurations examined are characterized by the same value of the Nusselt number. This may be explained by taking into account that the larger is the Rayleigh number, the more the fluid motion near a heated or a cooled sidewall is promoted mainly by the combined contributions of the sidewall itself and both adjacent horizontal surfaces, thus resulting substantially independent of the thermal boundary condition assumed at the opposite vertical wall. Actually, through a series of tests conducted by reducing the Rayleigh number step-size, it has been found that the Rayleigh number over which the values of Nu_v are practically the same is peculiar of the enclosure geometry, tending to reduce with increasing the aspect ratio of the cavity, that, for what is being considered here, plays the same role of the Rayleigh number.

4.2. Effects of the aspect ratio

Isotherm and streamline contour plots relevant to configurations AA, HA, HC and HH are depicted in Fig. 6 for $Ra = 10^5$ and aspect ratios $A = 0.66$ to 8.

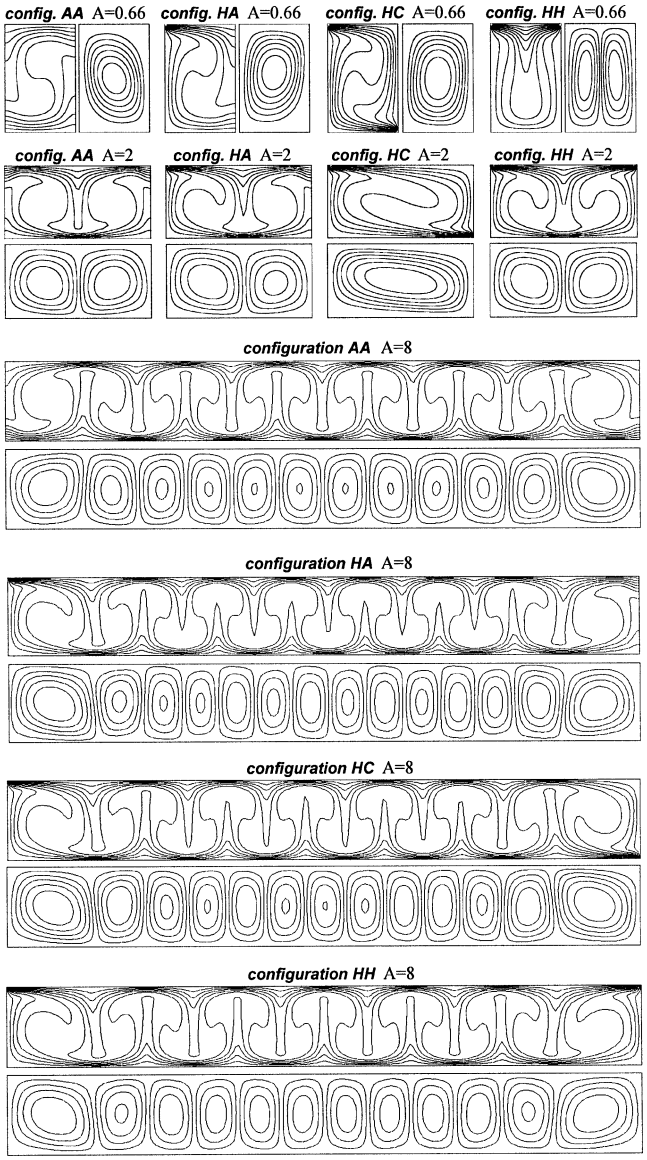

Fig. 6. Isotherms and streamlines for $Ra = 10^5$ and $0.66 \leqslant A \leqslant 8$.

It may be noticed that the number of cells of the flow field increases as the aspect ratio of the enclosure increases. In detail: (a) for configurations AA and HA a single-cell flow pattern remains stable as the aspect ratio increases from 0.66 to 1 (not represented), then turning into a multicell flow structure for aspect ratios $A \geqslant 2$; (b) for configurations HC and HH a single-cell flow pattern and a two-cell flow pattern, respectively, keep unaltered as the aspect ratio increases up to $A = 2$, over which the number of cells starts increasing. In addition: (a) for configuration AA the single-cell flow structure, and then the temperature distribution, is symmetric about the center of the enclosure, whilst the multicell patterns are symmetric about the vertical midplane of the cavity; (b) for configuration HA, as expected, the flow and thermal fields are always asymmetric; (c) for configurations HC and HH the velocity and temperature fields are always symmetric about the center of the enclosure and about the vertical midplane of the cavity, respectively.

The increase in the number of cells occurring as the aspect ratio of the cavity increases may be explained through the progressive breakdown of the density stratification in the fluid layers adjacent to the top and bottom walls that brings to the formation of alternating "columns" of hot and cold fluid travelling upward and downward across the cavity, with direct effects upon the temperature distribution.

As a matter of fact, such cell-splitting results in a spreading and a compression of the isotherms respectively near the base and the top of each ascending or descending column of hot or cold fluid, i.e., a spreading in the vicinity of the ceiling and a compression in the vicinity of the floor is observed next to the columns of fluid travelling downward, and vice versa for the columns of fluid travelling upward. It then follows that the temperature gradient on the bottom and top walls, and thus the corresponding heat flux, has a wave-type distribution directly related to the multicell flow structure occurring inside the cavity.

Furthermore, it seems worthwhile noticing that, for all the configurations analyzed, the outer cells located closer to either heated or cooled vertical sidewalls exert a compression of the inner cells. Such cell-compression propagates throughout the enclosure, thus influencing the local distribution of the isotherms and then the values of the local heat flux. The larger is the aspect ratio of the enclosure, the smoother is the propagation of the compression-related effects toward the middle of the cavity.

The distributions of the Nusselt numbers Nu_h and Nu_v relevant to $Ra = 10^5$ are plotted vs. the aspect ratio of the enclosure respectively in Figs. 7 and 8.

It may be observed that the heat transfer rates from the heated floor (or the cooled ceiling), starting from quite different values for the several configurations analyzed, tend asymptotically to the same value (typical of configuration AA) as the aspect ratio of the enclosure increases. This is due to the progressively more negligible influence of the thermal boundary conditions assumed at both sidewalls upon the temperature and flow fields. The "asymptotic" values obtained at the several Rayleigh numbers investigated are in good agreement with the experimental measurements carried out by Arnold et al. [16]. In addition, they are also consistent with the values that may be derived from the correlation-equation for natural convection heat transfer in horizontal air layers obtained by Hollands et al. from a wide set of experimental data [17]. Also the Nusselt numbers of the heated or cooled sidewalls, regardless of the configuration, tend to a unique constant value as the aspect ratio of the enclosure increases. This is again due to the fact that when the aspect ratio of the cavity is sufficiently large, the temperature distribution in the proximity of a heated or a cooled sidewall is practically independent of the boundary condition assumed at the opposite sidewall.

As concerns the cited tendency of the average horizontal Nusselt numbers to coincide as the aspect ratio of the cavity

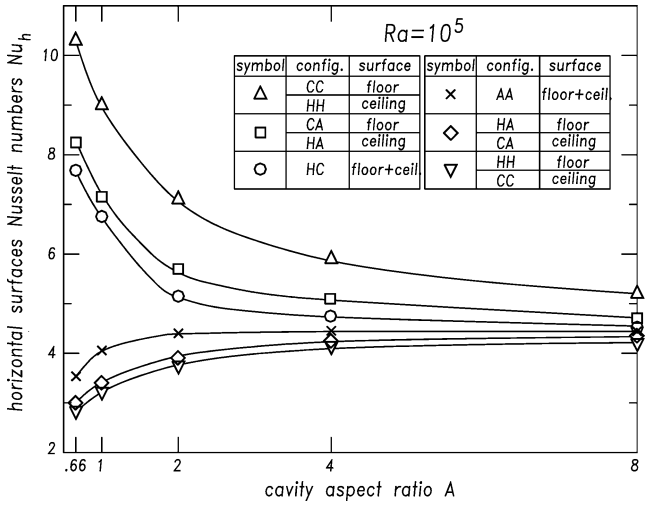

Fig. 7. Distributions of Nu_h vs. A for $Ra = 10^5$ (all configurations analyzed).

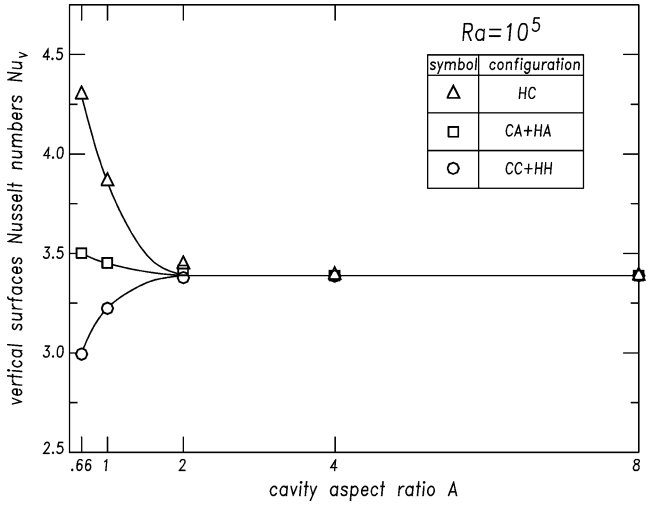

Fig. 8. Distributions of Nu_v vs. A for $Ra = 10^5$ (all configurations analyzed).

increases, it seems worthwhile noticing that, on the contrary, the local value of the Nusselt number is strictly dependent on the thermal boundary conditions assumed at both sidewalls. This is, e.g., the case of configurations HC and HH, as shown in Fig. 9, where, with reference to $A = 8$ and $Ra = 10^5$, the distributions of the local Nusselt number of the ceiling are reported vs. the dimensionless horizontal coordinate x/H. Indeed, it may be seen that at some locations the local Nusselt numbers pertaining to the thermal configurations considered may also differ by three to four times.

4.3. Heat transfer dimensionless correlations

The numerical results obtained for the average Nusselt numbers Nu_h and Nu_v defined in Eqs. (8) and (9) are expressed as a function of both the aspect ratio and the Rayleigh number of the enclosure through simple monomial correlations put in the general form $Nu = K A^{\alpha} Ra^{\beta}$.

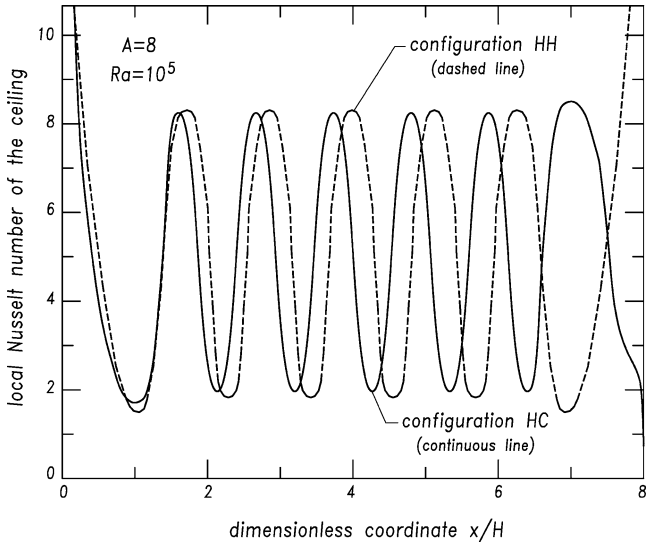

Fig. 9. Distributions of the local Nusselt number of the ceiling vs. x/H (configurations HC and HH).

For each boundary surface of any thermal configuration analyzed, the values of the coefficient K and both exponents α and β are evaluated by the least-square method through a logarithmic multiple regression procedure.

The dimensionless correlation-equations obtained from the best-fit of data in the ranges $0.66 \leqslant A \leqslant 8$ and $10^4 \leqslant Ra \leqslant 10^6$, are listed below together with the relevant standard deviation of data σ and the absolute value of the maximum relative error η.

Configuration AA

$$Nu_{\text{floor}}^{(\text{AA})} = Nu_{\text{ceiling}}^{(\text{AA})} = 0.210 A^{0.09} Ra^{0.25} \quad (\sigma = 0.041,\ \eta = 0.093) \tag{13}$$

Configurations HA and CA

$$Nu_{\text{floor}}^{(\text{CA})} = Nu_{\text{ceiling}}^{(\text{HA})} = 0.711 A^{-0.23} Ra^{0.20} \quad (\sigma = 0.032,\ \eta = 0.065) \tag{14}$$

$$Nu_{\text{ceiling}}^{(\text{CA})} = Nu_{\text{floor}}^{(\text{HA})} = 0.324 A^{0.12} Ra^{0.20} \quad (\sigma = 0.049,\ \eta = 0.089) \tag{15}$$

$$Nu_{\text{side}}^{(\text{CA})} = Nu_{\text{side}}^{(\text{HA})} = 0.650 A^{-0.03} Ra^{0.15} \quad (\sigma = 0.029,\ \eta = 0.080) \tag{16}$$

Configuration HC

$$Nu_{\text{floor}}^{(\text{HC})} = Nu_{\text{ceiling}}^{(\text{HC})} = 0.674 A^{-0.25} Ra^{0.20} \quad (\sigma = 0.061,\ \eta = 0.091) \tag{17}$$

$$Nu_{\text{sides}}^{(\text{HC})} = 0.526 A^{-0.09} Ra^{0.18} \quad (\sigma = 0.067,\ \eta = 0.115) \tag{18}$$

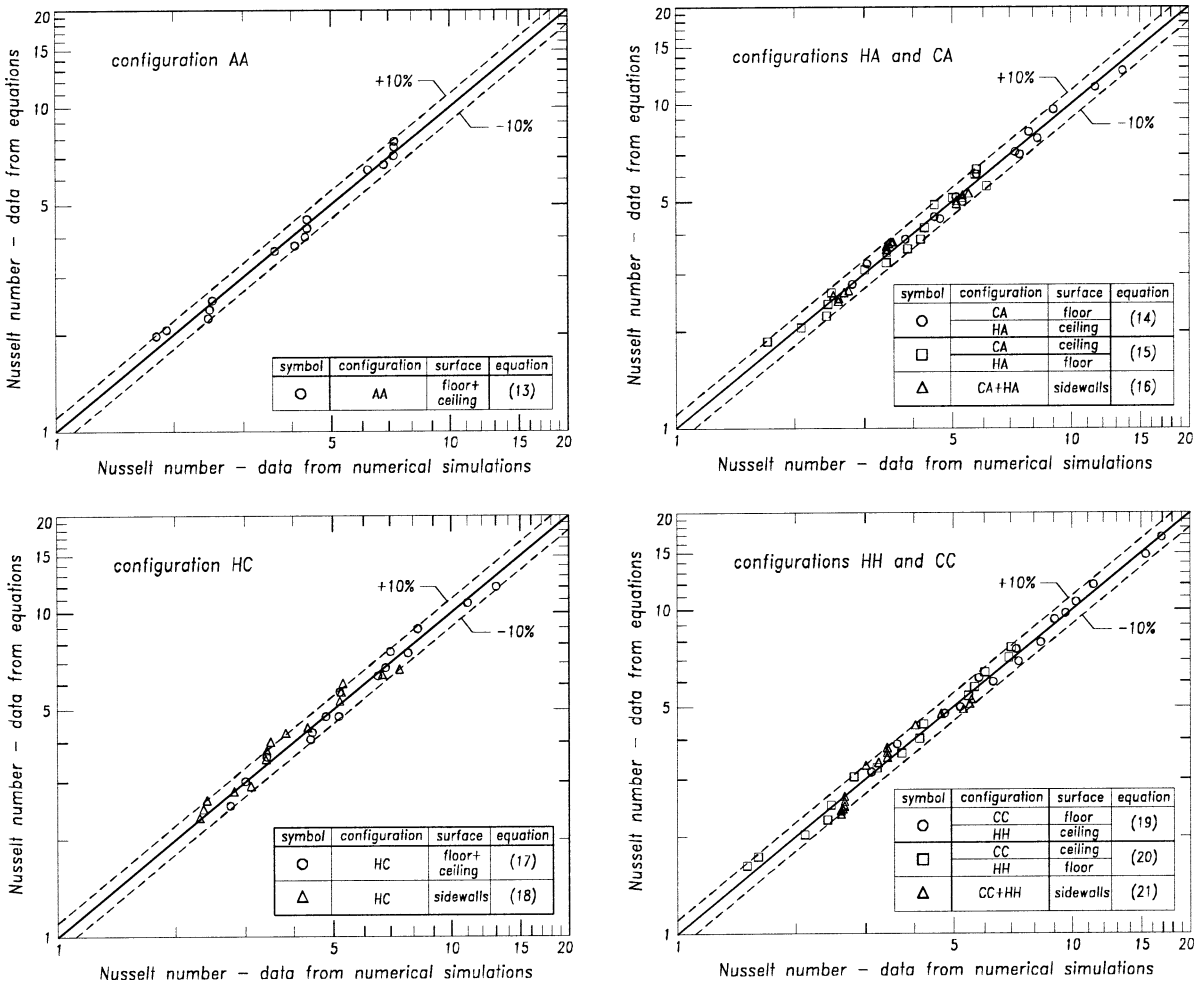

Fig. 10. Comparison between the Nusselt numbers predicted by Eqs. (13)–(21) and those derived from the numerical simulations.

Configurations HH and CC

$$Nu_{\text{floor}}^{(\text{CC})} = Nu_{\text{ceiling}}^{(\text{HH})} = 0.930A^{-0.30}Ra^{0.20} \quad (\sigma = 0.029,\ \eta = 0.058) \tag{19}$$

$$Nu_{\text{ceiling}}^{(\text{CC})} = Nu_{\text{floor}}^{(\text{HH})} = 0.182A^{0.15}Ra^{0.25} \quad (\sigma = 0.044,\ \eta = 0.082) \tag{20}$$

$$Nu_{\text{sides}}^{(\text{CC})} = Nu_{\text{sides}}^{(\text{HH})} = 0.590A^{0.05}Ra^{0.15} \quad (\sigma = 0.056,\ \eta = 0.090) \tag{21}$$

The comparison between the Nusselt numbers predicted by Eqs. (13)–(21) and those obtained through the numerical simulations performed is reported in Fig. 10 for all the configurations analyzed.

5. Conclusions

Natural convection heat and momentum transfer in air-filled, rectangular enclosures heated from the bottom and cooled from the top has been studied numerically for several specified thermal boundary conditions at the sidewalls, for width-to-height aspect ratios of the enclosure in the range between 0.66 and 8, and for values of the Rayleigh number based on the cavity height in the range between 10^3 and 10^6. Heat transfer dimensionless correlation-equations have been developed for each boundary surface of any thermal configuration investigated.

The main results obtained may be summarized as follows:

(a) with respect to the basic thermal configuration wherein the sidewalls are insulated, the heat transfer rate from the heated bottom wall (or the cooled top wall) increases as each adiabatic sidewall is replaced by a cooled (or a heated) sidewall, while showing only slight decreases as such replacement is carried out through a heated (or a cooled) sidewall;

(b) as usual, the heat transfer rate from any heated or cooled boundary surface of the enclosure increases as the Rayleigh number increases;

(c) each geometrical configuration of the enclosure is characterized by a specific value of the Rayleigh number over which the heat transfer rate from any heated or cooled sidewall is independent of the boundary condition assumed at the opposite sidewall;

(d) once the Rayleigh number is assigned, for all the thermal configurations investigated the heat transfer rates from the top and bottom walls tend asymptotically to the same value (typical of horizontal air layers) as the cavity aspect ratio increases;
(e) on the contrary, the local heat fluxes from the top and bottom walls are strictly dependent on the thermal boundary conditions assumed at both sidewalls;
(f) for cavity aspect ratios larger than a specific value that depends only on the Rayleigh number, the heat transfer rate from the heated or cooled sidewalls is independent of the thermal configuration of the enclosure.

References

[1] I. Catton, Natural convection in enclosures, in: Proceedings of the Sixth International Heat Transfer Conference, Toronto, Vol. 6, 1978, pp. 13–30.
[2] S. Ostrach, Natural convection in enclosures, J. Heat Transfer 110 (1988) 1175–1190.
[3] M. Ciofalo, T.G. Karayiannis, Natural convection heat transfer in a partially—or completely—partitioned vertical rectangular enclosure, Internat. J. Heat Mass Transfer 34 (1991) 167–179.
[4] R.B. Chinnokotla, D. Angirasa, R.L. Mahajan, Parametric study of buoyancy-induced flow and heat transfer from L-shaped corners with asymmetrically heated surfaces, Internat. J. Heat Mass Transfer 39 (1996) 851–865.
[5] M. November, M.W. Nansteel, Natural convection in rectangular enclosures heated from below and cooled along one side, Internat. J. Heat Mass Transfer 30 (1987) 2433–2440.
[6] A. Valencia, R.L. Frederick, Heat transfer in square cavities with partially active vertical walls, Internat. J. Heat Mass Transfer 32 (1989) 1567–1574.
[7] R. Anderson, G. Lauriat, The horizontal natural convection boundary layer regime in a closed cavity, in: Proceedings of the Eighth International Heat Transfer Conference, San Francisco, CA, Vol. 4, 1986, pp. 1453–1458.
[8] M.M. Ganzarolli, L.F. Milanez, Natural convection in rectangular enclosures heated from below and symmetrically cooled from the sides, Internat. J. Heat Mass Transfer 38 (1995) 1063–1073.
[9] O. Aydin, A. Unal, T. Ayhan, Numerical solutions for buoyancy-driven flow in a 2-D square enclosure heated from one side and cooled from above, in: Proceedings of the Advances in Computational Heat Transfer Symposium, Begell House, New York, 1997, pp. 387–394.
[10] O. Aydin, A. Unal, T. Ayhan, Natural convection in rectangular enclosures heated from one side and cooled from the ceiling, Internat. J. Heat Mass Transfer 42 (1999) 2345–2355.
[11] G.S. Shiralkar, L. Tien, A numerical study of the effect of a vertical temperature difference imposed on a horizontal enclosure, Numer. Heat Transfer 5 (1982) 185–197.
[12] A.T. Kirkpatrick, M. Bohn, An experimental investigation of mixed cavity natural convection in the high Rayleigh number regime, Internat. J. Heat Mass Transfer 29 (1986) 69–82.
[13] S.V. Patankar, Numerical Heat Transfer and Fluid Flow, Hemisphere, Washington, DC, 1980.
[14] A. Settari, K. Aziz, A generalization of the additive correction methods for the iterative solution of matrix equations, SIAM J. Numer. Anal. 10 (1973) 506–513.
[15] G. de Vahl Davis, Natural convection of air in a square cavity: A bench mark numerical solution, Internat. J. Numer. Meth. Fluids 3 (1983) 249–264.
[16] J.N. Arnold, I. Catton, D.K. Edwards, Experimental investigation of natural convection in inclined rectangular regions of differing aspect ratios, J. Heat Transfer (1976) 67–71.
[17] K.G.T. Hollands, G.D. Raithby, L. Konicek, Correlation equations for free convection heat transfer in horizontal layers of air and water, Internat. J. Heat Mass Transfer 18 (1975) 879–884.